Low Power Mach–Zehnder Modulator in Silicon-Organic Hybrid Technology

Robert Palmer, Luca Alloatti, Dietmar Korn, Philipp Claudius Schindler, Moritz Baier, Jens Bolten, Thorsten Wahlbrink, Michael Waldow, Raluca Dinu, Wolfgang Freude, Christian Koos, and Juerg Leuthold

***Abstract*— We report on a silicon-organic hybrid modulator based on a Mach–Zehnder interferometer (MZI) operating at 10 Gbit/s with an energy consumption of 320 fJ/bit. The device consists of a striploaded slot waveguide covered with an electro-optic polymer cladding. The MZI modulator is poled to be driven in push–pull operation by a single coplanar RF line. Our nonlinear coefficient $r_{33} = 15$ pm/V in combination with an 80 nm narrow slot enables RF peak-to-peak drive voltages as low as 800 mV_{pp} to suffice for an extinction ration of 4.4 dB for a 1.5 mm long modulator.**

***Index Terms*— Electrooptic modulators, photonic switching systems.**

I. Introduction

SILICON electro-optic modulators are key elements in telecommunications, data-communications and optical interconnects. So far, modulators were demonstrated based on free carrier depletion [1]–[3] or injection [4], [5] in diode structures or MOS (metal-oxide-semiconductor) structures [6]. Also the Pockels effect was exploited in silicon slot waveguides [7] using an electro-optic organic cladding [8]–[12] or in strained silicon rib-waveguides [13], [14]. A major challenge is to keep RF modulator voltages compatible with CMOS driver electronics, removing the need of power consuming RF amplifiers. Other important modulator parameters are device footprint, electrical and optical bandwidth, π-voltage-length product $V_\pi L$, extinction ratio, and energy consumption [15]. Resonant structures such as ring resonators [5], [16]–[18] can be operated with low drive voltages, and have a small foot-print as well, but their performance depends strongly on wavelength and operation temperature. For stabilization, energy consuming feedback loops are necessary, thereby limiting the field of application. In contrast, modulators based on Mach–Zehnder interferometers (MZI) have only weak temperature and wavelength dependency, but a larger footprint and a rather large operating voltage. Devices based on carrier depletion prove to be inferior to injection based devices in terms of length and operation voltage, but are superior in terms of bandwidth and energy-consumption [15]. Therefore, depletion based devices are usually preferred for high speed applications. Voltage-length products $V_\pi L$ are typically larger than 10 Vmm for nonresonant structures, while 7 Vmm has been reported for resonant structures [19], [20]. Extinction ratios (ER) are typically in the order of (3–8) dB at data rates above 20 Gbit/s [15]. At 10 Gbit/s ERs exceeding 10 dB have been demonstrated [21], [22]. To reduce the drive voltage of nonresonant depletion MZI modulators, the length of the phase modulator region can be extended to several millimeters. This way an MZI depletion modulator was reported featuring a length of 5 mm, a bias dependent $V_\pi L$ of 10...50 Vmm and 4.2 dB extinction ratio at 20 Gbit/s for a drive voltage of 1 V_{pp} when operated at quadrature [23].

Here we report of an MZI modulator based on the silicon-organic hybrid (SOH) approach [9]. Our MZI modulator has a short length of 1.5 mm, a voltage length product $V_\pi L$ of 2.7 Vmm and an extinction ratio of 4.4 dB measured at 10 Gbit/s for a drive voltage of 800 mV_{pp}. The low drive voltage will enable photonic-electronic integration without RF amplifiers and small footprint.

II. Silicon-Organic Hybrid Modulator

Silicon-organic hybrid devices combine conventional silicon-on-insulator (SOI) waveguides with functional organic cladding materials. The cross section of an SOH phase modulator is depicted in Fig. 1(a). It consists of two 240 nm wide silicon rails separated by an 80 nm wide slot. The dimensions have been verified with a scanning electron microscope, Fig. 1(b). The waveguide is covered by an organic electro-optic cladding. In this letter we used the electro-optic polymer M3 of GigOptix Inc. [24], which uniformely

Manuscript received February 11, 2013; revised April 6, 2013; accepted April 26, 2013. Date of publication April 30, 2013; date of current version June 18, 2013. This work was supported in part by the DFG Center for Functional Nanostructures, in part by the Karlsruhe School of Optics and Photonics, in part by the Helmholtz International Research School for Teratronics, in part by the DFG Major Research Instrumentation Programme, in part by the Alfried Krupp von Bohlen und Halbach Foundation, in part by the EU-FP7 Projects SOFI under Grant 248609 and PHOXTROT, in part by the BMBF joint project MISTRAL under Grant 01BL0804, and in part by the European Research Council Starting Grant "EnTeraPIC" (280145).

R. Palmer, L. Alloatti, D. Korn, P. C. Schindler, M. Baier, W. Freude, and C. Koos are with the Institute of Photonics and Quantum Electronics, Karlsruhe Institute of Technology, Karlsruhe 76131, Germany (e-mail: robert.palmer@kit.edu; luca.alloatti@kit.edu; korn@kit.edu; schindler@kit.edu; moritz.baier@student.kit.edu; wolfgang.freude@kit.edu; christian.koos@kit.edu).

J. Bolten, T. Wahlbrink, and M. Waldow are with AMO GmbH, Aachen 52074, Germany (e-mail: bolten@amo.de; wahlbrink@amo.de; waldow@amo.de).

R. Dinu is with EO Division, GigOptix Inc., Bothell, WA 98011 USA (e-mail: rdinu@gigoptix.com).

J. Leuthold was with the Institute of Photonics and Quantum Electronics, Karlsruhe Institute of Technology, Karlsruhe 76131, Germany. He is now with the Swiss Federal Institute of Technology, Zuerich CH-8093, Switzerland (e-mail: juergleuthold@ethz.ch).

Color versions of one or more of the figures in this letter are available online at http://ieeexplore.ieee.org.

Digital Object Identifier 10.1109/LPT.2013.2260858

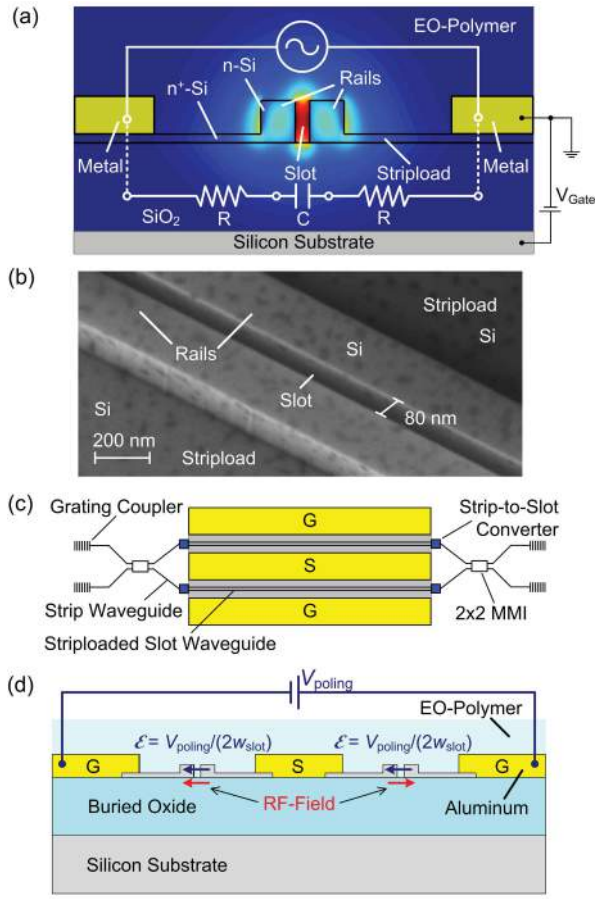

Fig. 1. (a) Schematic and simulation of the quasi-TE polarized mode of the phase modulator. The dominant electric field component is parallel to the substrate. Field discontinuities at the slot boundaries lead to a strong light confinement within the 80 nm wide slot. The two rails of the slot waveguide are electrically connected to metal electrodes by 45 nm thick n-doped (As, $1.5{\cdot}10^{17}\mathrm{cm}^{-3}$) silicon strips (stripload). In this way the applied potential predominantly drops across the 80 nm wide slot. This results in a high electric field in the slot and in a high overlap between optical and electrical mode. (b) SEM image of the striploaded slot waveguide. The measured slot width is 80 nm. The dark spots are residues of the polymer cladding. (c) Schematic of the device. The MZI consists of two phase modulators as described in (a) operated in push-pull configuration by a single coplanar line (GSG: ground – signal – ground) and two 2 × 2 multimode interference couplers (MMI). Light is coupled to the chip using grating couplers. (d) Cross section of the modulator. Schematic illustration of how the poling voltage is applied to achieve push-pull operation. The voltage source is connected to the two ground electrodes for poling. In that way half of the poling voltage drops across each slot and the global orientation of the chromophore dipoles in both phase modulators is identical.

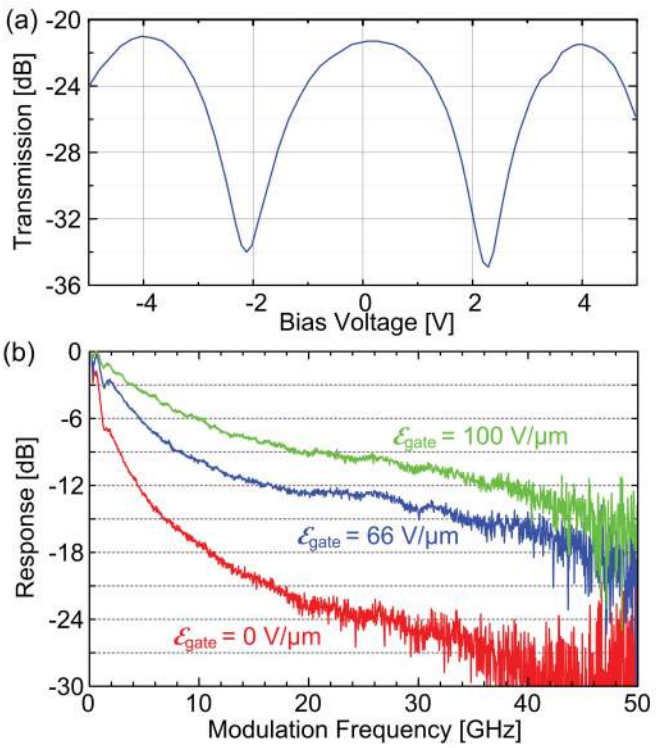

Fig. 2. Static and dynamic properties of the MZI modulator. (a) DC operation of the modulator with a gate field of 66 V/μm. Dependent on the operating point, a V_π between 1.8 V and 2.2 V is measured. (b) Electrical-optical-electrical response of the MZI modulator measured for 3 different gate fields. The gate field, see Fig. 1(a), has a strong impact on the modulator bandwidth indicating that the doping concentration in the silicon striploads is not sufficient for high speed operation. The gate field increases the conductivity of the striploads. At a field of 100 V/μm, the 6 dB bandwidth is 10 GHz. The bandwidth could be further enhanced by increasing the gate field. Dielectric breakdown of the SiO_2-layer occurs at 900 V/μm [28].

fills the slot. Discontinuities of the dominant (horizontal) electric field component at the slot sidewalls lead to a strong light confinement of the quasi-TE mode within the slot. The two rails of the slot waveguide are connected to a metal transmission line by 45 nm thick n-doped (As, $1.5 \cdot 10^{17}\mathrm{cm}^{-3}$) silicon strips (stripload). This way the applied voltage drops predominantly across the 80 nm wide slot. This results in a strong electric field that has a large overlap with the optical mode [8]. The conductivity of the striploads can be further enhanced by applying a gate-voltage V_{Gate} between silicon substrate and stripload, as depicted in Fig. 1(a). A more detailed description of the "gate-functionality" can be found in reference [12]. The schematic of the MZI modulator with multimode interference (MMI) couplers is depicted in Fig. 1(c). It consists of a balanced MZI and two identical 1.5 mm long SOH phase modulators, Fig. 1(a). The silicon waveguides were fabricated on an SOI wafer with a 220 nm thick device layer and a 3 μm thick buried oxide using a fabrication process similar to the one described in [25]. Grating couplers couple light from a single mode fiber to the silicon chip [26]. Strip waveguides are used as on-chip access waveguides. Efficient coupling between strip and striploaded slot waveguides is ensured by using logarithmically tapered mode converters [25]. A coplanar transmission line, consisting of 450 nm thick aluminum lanes, is used to drive the single-drive push-pull MZI modulator. The two phase modulators were poled at elevated temperatures with opposite polarities by applying the poling voltage across the ground electrodes of the coplanar transmission line as depicted in Fig. 1(d). In this way half of the applied poling voltage drops across each silicon slot. For poling, the sample is heated to 168 °C, and a poling voltage of 44 V (22 V per phase modulator) is applied. At room temperature, the poling current is in the nA-region indicating that both rails are well insulated.

III. Characterization

In this section static and dynamic properties of the modulator are investigated first. Then, on-off keying at a data rate of 10 Gbit/s is demonstrated.

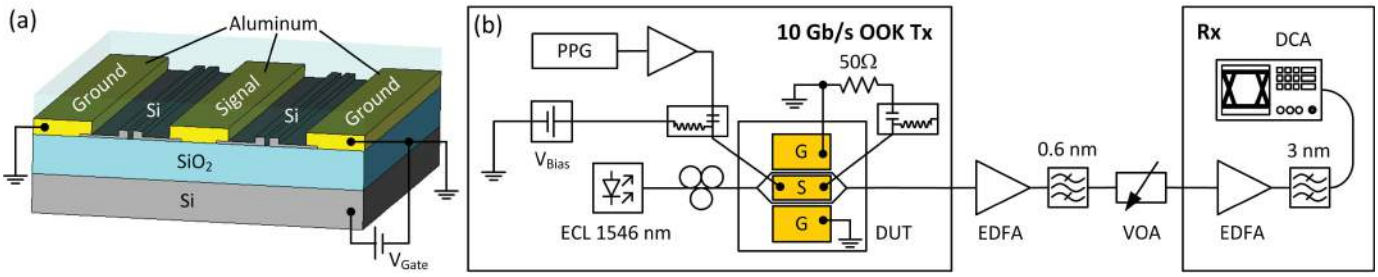

Fig. 3. (a) Schematic of the MZM. A gate field is applied through the substrate to increase the conductivity of the waveguides [12]. (b) Experimental setup. A 10 Gbit/s pseudorandom bit pattern generator (PPG) is used to drive the MZM. The signal is amplified and fed into the modulator using GSG-picoprobes. A bias voltage is applied over the same GSG electrodes by using a bias-T. A second picoprobe at the end of the modulator is used to terminate the electrical signal. Light from an external cavity laser (ECL) with controlled polarization at a wavelength of 1546 nm is coupled to the silicon chip using grating couplers. The signal is subsequently amplified and received by a digital communications analyzer (DCA).

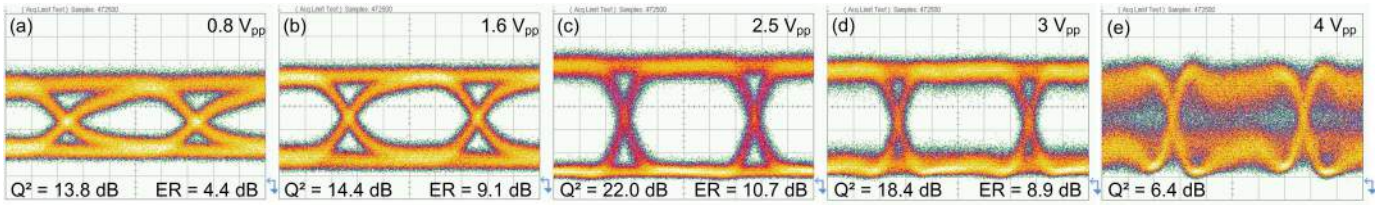

Fig. 4. 10 Gbit/s NRZ-OOK eye-diagrams measured at quadrature. At this data rate we find the π-voltage of the modulator to be 2.5 V_{pp}. Increasing the drive voltage to 3 V_{pp} or above leads to over-modulation. Open eye diagrams are also achieved when the drive voltage is reduced to 1.6 V_{pp} and 800 mV_{pp}. The measured Q^2-factors and extinction ratios (ER) are noted in the figure. 200 μV/div.

A. Modulator Properties

Static properties of the modulator are depicted in Fig. 2(a). A gate field of 66 V/μm is applied between the stripload and the substrate for increasing the conductivity of the striploads, Fig. 1(a). In Fig. 2(a) we depict the MZI characteristic as a function of the bias voltage. The V_π voltage is found to be dependent on the bias point: $V_\pi = 2.2$ V when biased with 1.3 V and $V_\pi = 1.8$ V when biased with 3.1 V. From these data, and with the waveguide dimensions $w_{\text{slot}} = 80$ nm, $w_{\text{rail}} = 240$ nm, $h_{\text{stripload}} = 45$ nm we calculate a nonlinear coefficient r_{33} of 15 pm/V, while the theoretically achievable value is 70 pm/V for this material [24]. For modulators with wider slots of 150 nm width higher nonlinear coefficients of 40 pm/V have been achieved. With another polymer cladding higher in-device coefficients of 58 pm/V have been reported [27], underlining the potential of the approach to further reduce drive voltages in the future. The electrical-optical-electrical (EOE) frequency response of the modulator is measured and depicted in Fig. 2(b). The measurement is performed with an electrical vector network analyzer, a CW laser, the device under test (DUT) and a high speed photodetector. If no gate field is applied, we observe that the bandwidth of the modulator is below 2 GHz, indicating that the conductivity of the doped striploads is not sufficient for high-speed operation for the chosen doping concentration [8]. When applying the gate field the stripload conductivity increases, boosting the 6 dB-bandwidth to 10 GHz for a field of 100 V/μm. The bandwidth could be further enhanced by increasing the gate field. An SiO_2 layer can stand voltages up to 900 V/μm [28]. System experiments are carried out at a gate field of 66 V/μm. For the 3 μm buried oxide this corresponds to a gate voltage of 200 V. Although this voltage is high it results in a negligible power consumption of less than 20 pW due to the perfect insulation properties of the oxide. Furthermore, an advanced modulator scheme, as reported in [12], reduces the gate voltage to 0.7 V by using a 10 nm top oxide with poly-silicon overlay for the same gate field of 66 V/μm. Alternatively, the gate field can be avoided by properly adjusting the doping concentration.

The fiber-to-fiber loss of the device is 21 dB with an on-chip loss of approximately 9 dB. This corresponds to an unexpected high loss of (5–6) dB/mm in the modulator section. We believe that this can be significantly improved in future, since measured losses in previously fabricated devices, based on the same fabrication scheme were as low as 1 dB/mm.

B. On-Off Keying Experiment

The modulator is tested in a system experiment as depicted in Fig. 3. A 10 Gbit/s signal is generated by a pseudorandom bit pattern generator (PPG), amplified and fed to the RF electrodes of the modulator using GSG picoprobes. To operate the modulator at quadrature a bias voltage of 3 V is applied via the same GSG electrodes using a bias-T. A second picoprobe at the end of the modulator terminates the electrical signal. Light at a wavelength of 1546 nm is coupled to the modulator from an external cavity laser (ECL) using grating couplers. The polarization is set to be quasi-TE polarization on the silicon chip. The modulated light leaving the DUT is amplified and received by a digital communications analyzer (DCA).

Recorded eye diagrams for various drive voltages are depicted in Fig. 4. A wide and open eye with an extinction ratio of 4.4 dB can be seen for a peak-to-peak drive voltage of 800 mV_{pp}, see Fig. 4(a). Increasing the drive voltage to 2.5 V_{pp} results in an optimum eye diagram with an extinction ratio of 11 dB and a high signal quality (Fig. 4(c), Q^2-factor

of 22 dB). Increasing the drive voltage to 3 V_{pp} and 4 V_{pp} leads to an over-modulation, Fig. 4(d,e).

In the current operation mode the drive signal is terminated in a 50 Ω resistor at the end of the modulator. Adding the energy dissipation in the resistor to the energy calculation results in an energy consumption of 320 fJ/bit for a drive voltage of 800 mV_{pp}. This value is among the lowest so far reported for a silicon MZI modulator at this data rate [15], [23]. Energy consumption due to gate voltage and bias voltage is below 1 aJ/bit. For a similar but shorter modulator of 1 mm length we verified that such devices can be operated without termination at data rates of up to 25 Gbit/s. Due to its short length the modulator acts as a "lumped" device at this data rate. Although the modulator used in this letter is 50% longer it is reasonable to assume that operation without termination at the reduced data rate of 10 Gbit/s is possible. With an ideal voltage source and without 50 Ω termination the energy consumption would be dominated by capacitive loading. For an on-chip drive voltage of 800 mV_{pp} and a calculated slot capacitance of $C = 189$ fF we estimate the energy consumption of the modulator per bit to be as low as $(1/4)(2C)V_{pp}^2 = 60$ fJ.

IV. Conclusion and Outlook

We have demonstrated a 1.5 mm long push-pull silicon-organic hybrid MZI modulator with a V_π of 1.8 V at DC and 2.5 V at a data rate of 10 Gbit/s, which corresponds to a polymer nonlinearity of $r_{33} = 15$ pm/V. Open eye diagrams and an extinction ratio of (4–11) dB are demonstrated for drive voltages as low as 800 mV_{pp} making electrical RF amplifiers dispensable. Improvements are possible concerning the poling procedure. With a fully poled structure the limit for V_π would be around 390 mV for this Mach–Zehnder structure and the chosen nonlinear polymer. The result forecasts ultra-low energy consuming electro-optic interconnects with silicon modulators directly driven by on-chip CMOS digital-to-analog converters.

Acknowledgment

The authors acknowledge technological support by the Karlsruhe Nano-Micro Facility (KNMF), by the Light Technology Institute (KIT-LTI) and the ePIXfab. They are grateful to Prof. D. Gerthsen (KIT-LEM) for support in nano-inspection and analysis. They acknowledge support by Deutsche Forschungsgemeinschaft and Open Access Publishing Fund of Karlsruhe Institute of Technology.

References

[1] P. Dong, *et al.*, "Low V_{pp}, ultralow-energy, compact, high-speed silicon electro-optic modulator," *Opt. Express*, vol. 17, no. 25, pp. 22484–22490, Dec. 2009.

[2] L. Liao, *et al.*, "40 Gbit/s silicon optical modulator for high-speed applications," *Electron. Lett.*, vol. 43, no. 22, pp. 1196–1197, Oct. 2007.

[3] D. J. Thomson, *et al.*, "50-Gb/s silicon optical modulator," *IEEE Photon. Technol. Lett.*, vol. 24, no. 4, pp. 234–236, Feb. 15, 2012.

[4] W. M. Green, M. J. Rooks, L. Sekaric, and Y. A. Vlasov, "Ultra-compact, low RF power, 10 Gb/s silicon Mach–Zehnder modulator," *Opt. Express*, vol. 15, no. 25, pp. 17106–17113, Dec. 2007.

[5] S. Manipatruni, Q. Xu, B. Schmidt, J. Shakya, and M. Lipson, "High speed carrier injection 18 Gb/s silicon micro-ring electro-optic modulator," *Lasers Electro-Opt. Soc.*, vol. 20, pp. 537–538, Oct. 2007.

[6] J. Fujikata, *et al.*, "25 GHz operation of silicon optical modulator with projection MOS structure," in *Proc. Opt. Fiber Commun. Conf.*, Mar. 2010, pp. 1–3.

[7] V. R. Almeida, Q. F. Xu, C. A. Barrios, and M. Lipson, "Guiding and confining light in void nanostructure," *Opt. Lett.*, vol. 29, no. 11, pp. 1209–1211, Jun. 2004.

[8] J.-M. Brosi, C. Koos, L. C. Andreani, M. Waldow, J. Leuthold, and W. Freude, "High-speed low-voltage electro-optic modulator with a polymer-infiltrated silicon photonic crystal waveguide," *Opt. Express*, vol. 16, no. 6, pp. 4177–4191, Mar. 2008.

[9] J. Leuthold, *et al.*, "Silicon organic hybrid technology—A platform for practical nonlinear optics," *IEEE Proc.*, vol. 97, no. 7, pp. 1304–1316, Jul. 2009.

[10] J. H. Wuelbern, *et al.*, "40 GHz electro-optic modulation in hybrid silicon-organic slotted photonic crystal waveguides," *Opt. Lett.*, vol. 35, no. 16, pp. 2753–2755, Aug. 2010.

[11] R. Ding, *et al.*, "Sub-volt silicon-organic electro-optic modulator with 500 MHz bandwidth," *J. Lightw. Technol.*, vol. 29, no. 8, pp. 1112–1117, Apr. 15, 2011.

[12] L. Alloatti, *et al.*, "42.7 Gbit/s electro-optic modulator in silicon technology," *Opt. Express*, vol. 19, no. 12, pp. 11841–11851, Jun. 2011.

[13] R. S. Jacobsen, *et al.*, "Strained silicon as a new electro-optic material," *Nature*, vol. 441, pp. 199–202, May 2006.

[14] B. Chmielak, *et al.*, "Pockels effect based fully integrated, strained silicon electro-optic modulator," *Opt. Express*, vol. 19, no. 18, pp. 17212–17219, Aug. 2011.

[15] G. T. Reed, G. Mashanovich, F. Y. Garde, and D. J. Thomson, "Silicon optical modulators," *Nature Photon.*, vol. 4, pp. 518–526, Aug. 2010.

[16] C. A. Barrios, V. R. Almeida, R. Panepucci, and M. Lipson, "Electrooptic modulation of silicon-on-insulator submicrometer-size waveguide devices," *J. Lightw. Technol.*, vol. 21, no. 10, pp. 2330–2332, Oct. 2003.

[17] L. Chen, K. Preston, S. Manipatruni, and M. Lipson, "Integrated GHz silicon photonic interconnect with micrometer-scale modulators and detectors," *Opt. Express*, vol. 17, no. 17, pp. 15248–15256, Aug. 2009.

[18] J. C. Rosenberg, *et al.*, "Low-power 30 Gbps silicon microring modulator," in *Proc. Quantum Electron. Laser Sci. Conf.*, May 2011, p. PDPB9.

[19] P. Dong, *et al.*, "High-speed and compact silicon modulator based on a racetrack resonator with a 1 V drive voltage," *Opt. Lett.*, vol. 35, no. 19, pp. 3246-3248, Oct. 2010.

[20] J. Rosenberg, *et al.*, "A 25 Gbps silicon microring modulator based on an interleaved junction," *Opt. Express*, vol. 20, no. 24, pp. 26411–26423, Nov. 2012.

[21] D. Thomson, *et al.*, "High contrast 40 Gbit/s optical modulation in silicon," *Opt. Express*, vol. 19, no. 12, pp. 11507–11516, Jun. 2011.

[22] K. Ogawa, *et al.*, "Silicon Mach–Zehnder modulator of extinction ratio beyond 10 dB at 10.0-12.5 Gbps," *Opt. Express*, vol. 19, no. 26, pp. B26–B31, Dec. 2011.

[23] T. Baehr-Jones, *et al.*, "Ultralow drive voltage silicon traveling-wave modulator," *Opt. Express*, vol. 20, no. 11, pp. 12014–12020, May 2012.

[24] D. Jin, H. Chen, A. Barklund, J. Mallari, G. Yu, E. Miller, and R. Dinu, "EO polymer modulators reliability study," *Proc. SPIE, Org. Photon. Mater. Devices XII*, vol. 7599, Mar. 2010.

[25] R. Palmer, *et al.*, "Low-loss silicon strip-to-slot mode converters," *Photon. J.*, vol. 5, no. 1, pp. 2200409-1–2200409-3, Feb. 2013.

[26] D. Taillaert, *et al.*, "Grating couplers for coupling between optical fibers and nanophotonic waveguides," *Jpn. J. Appl. Phys.*, vol. 45, pp. 6071–6077, Aug. 2006.

[27] X. Wang, C.-Y. Lin, S. Chakravarty, J. Luo, A. K.-Y. Jen, and R. T. Chen, "Effective in-device r33 of 735 pm/V on electro-optic polymer infiltrated silicon photonic crystal slot waveguides," *Opt. Lett.*, vol. 36, no. 6, pp. 882–884, Mar. 2011.

[28] C. M. Osburn and D. W. Ormond, "Dielectric breakdown in silicon dioxide films on silicon: II. Influence of processing and materials," *J. Electrochem. Soc.*, vol. 119, no. 3, pp. 597–603, Mar. 1972.